

1 **The atmospheric carbon sequestration potential of man-made tidal lagoons**

2

3 **Marco Piano^{a*}, Stathys Papadimitriou^{b1}, Ronan Roche^a, David Bowers^b, Paul**

4 **Kennedy^b, Hilary Kennedy^b**

5

6 *corresponding author: m.piano@bangor.ac.uk

7

8 ^aCentre for Applied Marine Science (CAMS), Bangor University, Menai Bridge,

9 Anglesey, LL59 5AB United Kingdom

10 ^bSchool of Ocean Sciences (SOS), Bangor University, Menai Bridge, Anglesey, LL59

11 5AB United Kingdom

12 *The authors confirm that there are no known conflicts of interest associated with this*
13 *publication and there has been no significant financial support for this work that could have*
14 *influenced its outcome.*

15 **Abstract**

16 Understanding sequestration of carbon by coastal ecosystems is central to addressing
17 the role they play in climate change mitigation. To quantify this process, accurate
18 measurements of CO₂ fluctuation, coupled with variations in residence time of coastal
19 water-bodies are required. Nearshore ecosystems, including coastal lagoons, may
20 provide an effective sink for atmospheric carbon dioxide, particularly those containing
21 productive biota such as seagrass. However, the rate and pattern of carbon
22 sequestration in seagrass meadows across a range of environmental settings is still
23 poorly constrained. In this study, we utilize a robust physical tidal model, along with
24 biogeochemical dissolved inorganic carbon (DIC) assessment, to estimate water
25 residence time and net sequestration of atmospheric CO₂ in an intertidal lagoon
26 containing a seagrass (*Zostera noltii*) meadow. Total alkalinity and pH measurements
27 taken from advected water mass exchanged with the open ocean at inlet boundaries
28 are used to calculate DIC and pCO₂. A predictive model of hydrodynamics provides
29 good approximation of mean water residence time to within 6 hr (\pm 3 s.d). Results
30 indicate that during the daytime study period the lagoon is a sink for carbon, having a
31 mean net ecosystem productivity (NEP) of 3.0 ± 0.4 mmol C m⁻² hr⁻¹. An equivalent diel
32 NEP range of between 15.23 and -9.24 mmol C m⁻² d⁻¹ is calculated based on reported
33 shallow water pelagic respiration rates. Moreover, approximately 4% of DIC availability
34 occurs from atmospheric CO₂ transfer to lagoon water. However, a negative diel rate of
35 -82 ± 81 mmol C m⁻² d⁻¹ is found, assuming overnight respiration ascertained from
36 converted *Zostera noltii* O₂ utilization. We hypothesize that analogous regional

1. Ocean Technology and Engineering, National Oceanography Centre, European Way, Southampton, SO14 3ZH United Kingdom

37 nearshore ecosystems provide baseline study sites suitable to elucidate the carbon
38 capture potential of planned, nearby tidal range energy schemes.

39 **Keywords**

40 Coastal lagoons; Atmosphere-ocean carbon exchange; Tidal energy; Carbon sinks;
41 Dissolved Inorganic Carbon; Irish Sea coastal modelling

42 **1. Introduction**

43 Coastal lagoons, saline ponds and barrier systems occupy around 13% of
44 coastal areas worldwide and accommodate important productive habitats such as
45 seagrass meadows (Barnes, 1989). Despite their sparse ocean coverage (<0.2%),
46 seagrass meadows play an important role in carbon sequestration and burial,
47 estimated to be between 20 and 112 Tg C yr⁻¹ (Duarte et al., 2010; Kennedy et al.,
48 2010; Fourqurean et al., 2012). However, not all seagrass meadows are net
49 autotrophic (Duarte et al., 2010); many nearshore coastal ecosystems are thought to
50 contribute to atmospheric CO₂ levels by acting as a net source, with heterotrophic
51 processes that produce CO₂ outweighing autotrophic processes that consume it (Mork
52 et al., 2016). Coastal lagoons can be productive environments due to high nutrient
53 levels in both sediments and water, and are frequently colonized by benthic plants due
54 to suitable sunlight penetration in the shallow water column. They represent a valuable
55 resource for both fisheries and blue carbon initiatives, supported by research finding
56 that shallow water autotrophic biota provide a functional sink for atmospheric CO₂
57 (Tokoro et al., 2014).

58 Current global carbon budgets show a deficit that is unattributed of 0.6 Gt C yr⁻¹
59 (Le Quere et al., 2018). The oceanic sink of anthropogenic CO₂ for the period 2002 to
60 2011 is estimated at 2.5 ± 0.5 Pg C yr⁻¹ (Le Quere et al., 2013), with oceanographers
61 researching understudied parts of the ocean, such as marginal seas and nearshore
62 ecosystems as potential missing sinks. Bauer et al. (2013) and Borges et al. (2005)
63 suggest (with some uncertainty) that temperate marginal seas may reduce atmospheric
64 CO₂ by some 0.45 Pg C yr⁻¹, with nearshore wetland and estuarine ecosystems almost
65 nullifying this sink by emitting around 0.35 to 0.40 Pg C yr⁻¹. It is suggested that future
66 research should focus on increasing high resolution carbonate system parameter data
67 (Mork et al., 2016) in highly productive nearshore systems, such as those containing
68 seagrass (Borges et al., 2005; Dai et al., 2009; Jiang et al., 2011). Tidal range power
69 schemes, such as the proposed Swansea Bay tidal lagoon^A may provide an
70 opportunity to fabricate carbon-sequestering nearshore ecosystems that increase the
71 potential to offset atmospheric carbon deficits.

^A <http://www.tidallagoonpower.com/projects/swansea-bay/>

72 Roche et al. (2016) suggest that accurate resource assessments relating to
73 marine renewable energy (MRE) schemes are required to elucidate physical,
74 ecological and social uncertainties when spatially refining developments to help
75 achieve carbon reduction targets. Tidal lagoons provide an important potential
76 resource for the MRE development mix, being both a predictable and controllable
77 renewable energy source. The feasibility and scope of planned UK tidal lagoon energy
78 schemes has undergone extensive examination by the 'Hendry Review'. However,
79 uncertainty exists as to their future, given the high initial capital costs involved and
80 possible inability to produce electricity at a competitive price. Additional benefits, such
81 as regeneration, recreational activities and flood protection are suggested (Neill et al.,
82 2018; NIC, 2018), however, the opportunity to incorporate carbon offsetting might also
83 provide a second potential revenue source, increasing financial feasibility.

84 A naturally restricted lagoon is defined as having two or more frictional inlets,
85 with definite tidal regimes, whereas choked lagoons characteristically have one or
86 more long narrow inlets with greater water residence time (Kjerfve, 1986). Residence
87 time is a quantitative measure allowing spatial and temporal estimation of the rate at
88 which water mass ingresses and egresses a control domain. It is effectively the time
89 taken for a particle entering the domain to leave again for the first time (Delhez et al.,
90 2014). Ecosystem issues such as depletion in fish production have been related to
91 limited seawater circulation and renewal (Tsihrintzis et al., 2007), because flushing has
92 a limiting impact on nutrient input (Newton and Mudge, 2005). Salt concentration, along
93 with nutrient and alkalinity balance may be reduced by inputs of freshwater from
94 surface run-off, contributories, heavy and prolonged precipitation or by evaporation. It
95 should be noted that larger lagoon systems are characteristically more stable and likely
96 to encourage species diversity (Barnes, 1989). Ultimately, water balance, composition
97 and quality depends on exchange at boundaries and the resultant residence time
98 (Orfila et al., 2005; Rynne et al., 2016).

99 Coastal lagoons are important areas for autotrophic processes resulting in net
100 carbon accumulation in sediments but are susceptible to anthropogenic impacts.
101 Industrial activities such as fossil fuel combustion and cement manufacturing have
102 increased atmospheric CO₂ concentration, influencing water pH. Terrestrial
103 deforestation and habitat clearing have created aquatic imbalances known as cultural
104 eutrophication and siltation, often manifested by increased turbidity, algal production,
105 decreased light availability and dissolved oxygen levels (Kennedy and Bjork, 2009;
106 Zouiten et al., 2013). Ultimately, this may cause loss of benthic plants and oxidation of
107 sediments leading to net heterotrophic activity, causing the lagoon to act as a carbon
108 source rather than a sink. It is, therefore, important to be able to robustly model carbon
109 dynamics in order to assess whether ecosystems are CO₂ sources or sinks.

110 In this study, we provide a method to quantify simply and robustly mean lagoon
111 NEP rates based on observed boundary flux estimates of DIC and modelled water
112 exchange through the tidal channels. The study site has restricted water exchange with
113 the open ocean through man-made inlets and is located in the vicinity of proposed sites
114 for tidal lagoon power schemes that will follow similar water exchange regimes. As
115 such similar regional ecosystems may provide analogous baseline study sites for
116 proposed MRE schemes. A physical-chemical box model approach provides volumetric
117 water exchange estimates at lateral boundaries from simulations provided by a one-
118 dimensional (1-D) MATLAB model. Modelled hydrodynamics are well validated; thus,
119 errors are constrained. Biogeochemical field measurements along with meteorological
120 data allow air-sea CO₂ transfer rates to be estimated over a complete tidal cycle. This
121 short-term study demonstrates the utility of this approach and identifies the potential for
122 annual carbon budgeting in semi-enclosed productive coastal lagoons using high-
123 resolution temporal data.

124

125 **2. Methods**

126 **2.1 Study site**

127 Sampling occurred in the Inland Sea (53°16.475'N, 4°35.000'W), a small (radius
128 and surface area at low tide ~890 m and 2.5 km², respectively), shallow (~2 m at low
129 tide), temperate, micro-tidal (<2 m range) coastal lagoon. The nearshore ecosystem is
130 sandwiched between road and rail embankments in a channel that separates Holy
131 Island from the island of Anglesey in Wales, UK (Figure 1). The lagoon was formed in
132 the early 19th century when Stanley Embankment (water inlet ~17 m wide and 100 m
133 long) was constructed to provide a transport route through to Holyhead. At the opposite
134 end of the lagoon, Four Mile Bridge provides a much narrower road bridge and
135 passage for water to enter (~6 m wide by 10 m long). The area is both a designated
136 Landscape Character Area (LCA) and Area of Outstanding Natural Beauty (AONB) and
137 provides an important well-balanced nursery and ecosystem for many different fish and
138 marine plant species. Further detail on the area is provided by Hill (1994).

139 Seawater exchange with the Irish Sea occurs through the two narrow man-
140 made inlets in the embankments. The hydrodynamic regime of the lagoon is dominated
141 by semi-diurnal advective mixing of seawater at lateral boundaries. Periodic tidal
142 forcing outside the basin is choked by the restricted inlets so that the tide in the Inland
143 Sea has a lower amplitude than that of the open ocean (Hill, 1994). The lagoon
144 supports a meadow of *Zostera noltii*, a small seagrass species of the intertidal zone of
145 Europe and Africa (Auby and Labourg, 1996). This species exhibits strong seasonality
146 in its above-ground biomass, ranging from 0.4 g DW m⁻² in spring to 70 g DW m⁻² in
147 summer (Papadimitriou et al., 2006). There are a number of proposed MRE

148 developments for this region, including a tidal range lagoon scheme to the east at
 149 Colwyn Bay (Roche et al., 2016).
 150

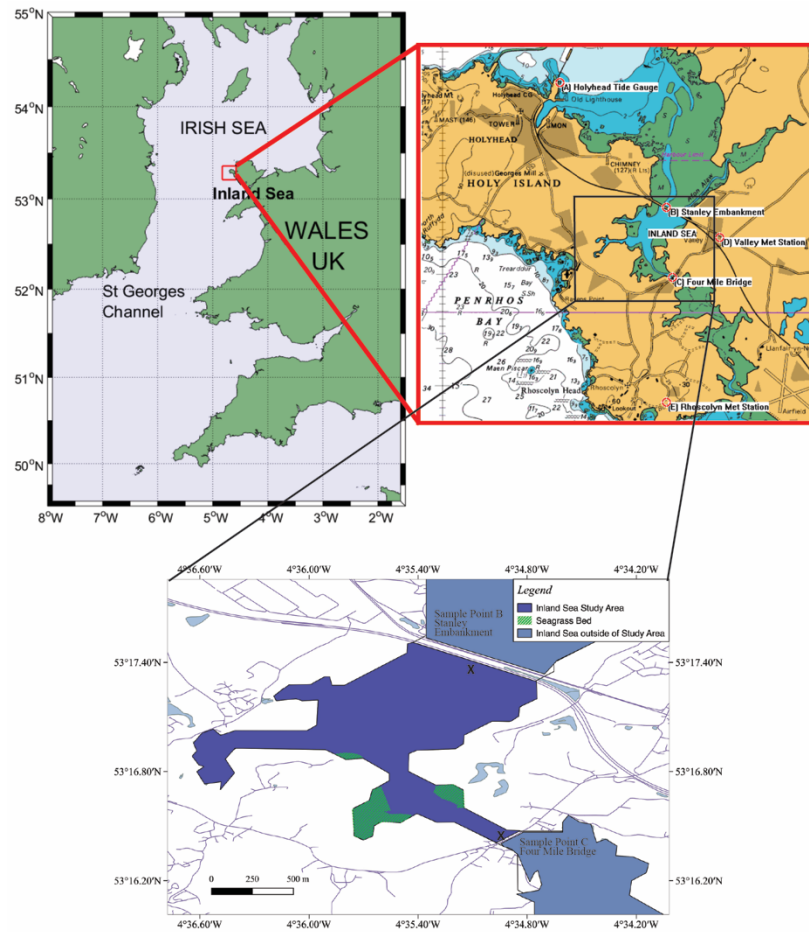


Figure 1. Location of the Inland Sea showing the restricted channels to the north at Stanley Embankment (B) and to the south at Four Mile Bridge (C). Modelled boundary conditions are based on data supplied by Holyhead harbour primary tide gauge station (A) and meteorological data is taken from stations at Valley (D) and Rhoscolyn (E).

151

152 2.2 Biogeochemical model

153 A simple theoretical 1-D biogeochemical model, adapted from Jiang et al.
 154 (2011) (Figure 2) is used to examine the extent to which lagoon DIC concentration is
 155 influenced by CO₂ gas exchange caused by a combination of:

- 156 (i) air-sea exchange (surface boundary)
- 157 (ii) physical mixing (lateral boundary)
- 158 (iii) biological influences (seabed and water column)

159

160 DIC determination is outlined in section 2.4. We apply the fundamental principles of a
 161 tracer (in this case DIC) entering and exiting a semi-enclosed study system and assume (a)
 162 lagoon volume is conserved and (b) a fully mixed water column. Therefore, tracer
 163 concentration (c , in mmol C kg^{-1}) in a varying water depth over time is given by eq (1)
 164 (Williams and Fellows, 2011):

165

$$\frac{d}{dt} \rho c \frac{V}{A_S} = \sum F_{out} - F_{in} = F_{MIX} - F_{GAS} - F_{BIO} \quad (1)$$

166

167 In the above equation, ρ is water density (kg m^{-3}), V system volume (m^3), A_S surface
 168 area (m^2), and F is the tracer flux ($\text{mmol C m}^{-2} \text{hr}^{-1}$) entering (F_{in}) and exiting (F_{out}) the
 169 system at the boundaries. DIC fluxes in and out of the lagoon can further be expressed
 170 as the sum of the partial fluxes generated by a number of biogeochemical processes
 171 within the lagoon:

- 172 (i) Physical mixing during transport by advection over ebb and flood tidal cycles,
 173 riverine input, and upwelling (F_{MIX}).
- 174 (ii) Ecosystem respiration, adding respired organic carbon as CO_2 to the water,
 175 and ecosystem production removing DIC species (aqueous CO_2 , bicarbonate
 176 ions) from the water into biomass and calcium carbonate (CaCO_3) precipitation
 177 and dissolution, combined as F_{BIO} .
- 178 (iii) Air-sea exchange of CO_2 (F_{GAS}). If $F_{in} > F_{out}$, there will be a net increase in DIC
 179 concentration in the lagoon water, and vice versa.

180

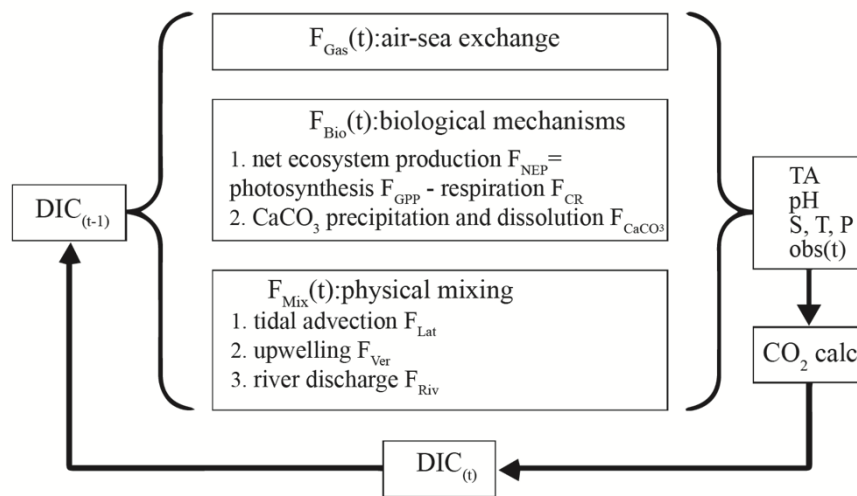


Figure 2. Biogeochemical 1-D model of carbonate system exchange dynamics when accounting for associated air-sea gas exchange, biological activity and physical processes in a nearshore shallow water ecosystem.

181

182 2.2.1 Biological processes

183 We simplify the approach to carbon dynamics in the lagoon by considering a
 184 semi-enclosed system (Figure 3). At first approximation, we assume that the
 185 contribution from CaCO_3 precipitation and dissolution is negligible (Barron et al., 2006).
 186 Based on eq (1), at steady state F_{BIO} is equivalent to NEP, the balance between gross
 187 primary production and community respiration, $F_{BIO} = \text{NEP} = \text{GPP} + \text{CR}$. By

188 convention, the transfer of carbon from atmosphere to seawater and lagoon to ocean
 189 due to respiration have negative values.
 190

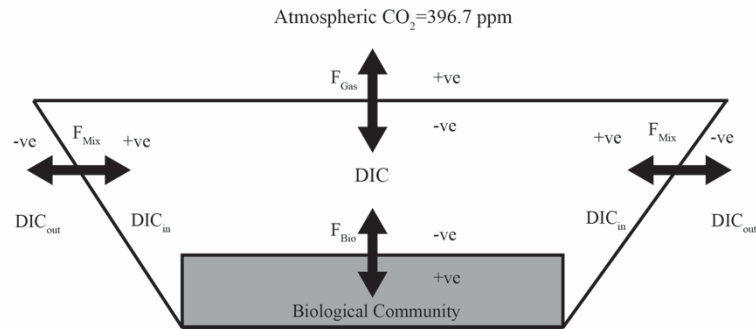


Figure 3. Schematic box model of the Inland Sea and its perceived inorganic carbon exchange. Lateral tidal mixing (Mix), biological (Bio) and gas (Gas) exchanges will drive net DIC concentration levels within the lagoon.

191

192 2.2.2 Air-sea exchange

193 In this study, we determine F_{GAS} with the bulk formula method as $F_{GAS} =$
 194 $\alpha k \Delta p CO_2$. Where α is the solubility coefficient of CO_2 ($mmol\ m^{-3}\ \mu atm^{-1}$), k is gas
 195 transfer velocity ($m\ hr^{-1}$; a function of wind speed) and $\Delta p CO_2 = pCO_{2W} - pCO_{2A}$ (μatm),
 196 the air-sea difference in the partial pressure of CO_2 . Subscripts W and A refer to water
 197 and atmosphere respectively.

198

199 2.2.3 Physical mixing

200 By observing any two of the four measurable carbonate system parameters,
 201 pH, DIC, total alkalinity (TA) and pCO_2 , along with water temperature and salinity, it is
 202 possible to determine the remaining parameters. In this study, DIC in lagoon water is
 203 determined from field observations of pH and TA at lateral boundaries. The physical
 204 processes of tidal advection, upwelling, and river discharge contribute to DIC mixing at
 205 ecosystem boundaries. Advection of nutrients from ocean tides dominate the Inland
 206 Sea, no other significant contributories exist. The tidal exchange of water through the
 207 man-made inlets provides fluxes calculated from the product of volumetric flow
 208 throughput, U ($m^3\ hr^{-1}$) and water density. The mixing of lagoon and ocean water
 209 includes tracer concentration, such that $F_{MIX} = c_L \rho U_{out} - c_O \rho U_{in}$ whereby subscripts *in*
 210 and *out* describe exchange on flood and ebb tides and subscripts *L* and *O* indicate
 211 lagoon and ocean concentrations, respectively.

212

213 2.3 Hydrodynamic model

214 The hydrodynamic model provides a means to estimate volumetric channel
 215 throughput, U . Following Hill (1994), the tide in the Inland Sea is modelled by

216 considering the balance between the pressure gradient force caused by the slope of
 217 the water surface and bottom friction:
 218

$$g \frac{\eta_o - \eta_L}{L} = k_D \frac{u^2}{H + \eta_m} \quad (2)$$

219
 220 Where g is the gravitational acceleration constant (9.81 m s^{-2}), η_o is surface elevation
 221 relative to mean sea level in the open sea (m), and η_L is surface elevation relative to
 222 mean sea level in the lagoon (m). The depth-averaged along-channel current velocity u
 223 (m s^{-1} , positive when flow is into the lagoon), and k_D the dimensionless drag coefficient
 224 in a channel of length L and depth H below mean sea level (m). Mean surface
 225 elevation in the channel is denoted by $\eta_m = (\eta_o + \eta_L) / 2$. The continuity equation is:
 226

$$A_S \frac{d\eta_L}{dt} = ub(H + \eta_m) \quad (3)$$

227
 228 and we consider ideal channels of width b (m), whose cross section does not alter.
 229 Crucially, however, in addition we allow the surface area of the lagoon to change with
 230 the tide, assuming the lagoon has sloping sides and a conical shape. If the sides slope
 231 at an angle θ ($^\circ$) to the horizontal, the surface area of the lagoon varies with elevation
 232 according to:
 233

$$A_S = \pi \left(r_0 + \frac{\eta_L}{\tan \theta} \right)^2 \quad (4)$$

234
 235 The subtidal lagoon radius, r_o (m) is that at lowest-tide, assumed constant with depth
 236 beyond this.

237 Tidal forcing in the open sea can be represented by a sum of harmonics:
 238

$$\eta_o = \sum_{n=1}^N a_n \cos(\omega_n t - \kappa_n) \quad (5)$$

239
 240 Where a_n and κ_n are the amplitude (m) and phase ($^\circ$) of n (1-N) tidal constituents with
 241 an angular frequency $\omega_n = \frac{2\pi}{T_n}$ with T_n being the period (s) of the constituent. For this
 242 study, twelve of the main harmonic constituents are used to represent surface
 243 elevation change due to astronomical forcing. Tidal boundary forcing at the Inland Sea

244 is assumed to occur at the same phase and amplitude as that at Holyhead harbour (A
 245 in Figure 1). The flow in the channels is derived by solving eq (2) for u and then using
 246 eq (3) to update the elevation in the Inland Sea. The equations are solved using a
 247 thirty-second-time step with meteorological influences neglected. U is derived from the
 248 product of channel flow velocity and cross-sectional area, which varies with depth over
 249 time.

250

251 **2.4 Water residence time and NEP**

252 Water exchange and mixing through the channels will not occur instantly and
 253 concentrations due to mixing will alter slowly and be affected by a proportion of water
 254 returning into the domain soon after leaving. Therefore, the average residence time of
 255 the water must be factored into calculations. In order to account for this mixing
 256 process, we approach the problem using the tracer pulse method that associates the
 257 residence time (T) of a system (in this case the lagoon basin) with n measured tracer
 258 flux concentration observations (F_{tr}) at any given point on the periphery during an
 259 elapsed time (t) by means of the transport equation:

260

$$T = \frac{\sum_{n=0}^{\infty} F_{tr} t}{\sum_{n=0}^{\infty} F_{tr}} \quad (6)$$

261

262 We solve the steady state condition of eq (6) by integrating over time the multiple
 263 tracer DIC flux observations to reveal the solution to tracer transport for a time step
 264 equal to a tidal cycle:

265

$$NEP = \frac{1}{T_{TC}} \int_0^{TC} F_{MIX} - F_{GAS} dt \quad (7)$$

266

267 Water residence time during a tidal cycle (T_{TC}) is the ratio of the mean volume of the
 268 lagoon V_L , (m^3) to the tidal prism volume, V_{TP} , ($m^3 \text{ hr}^{-1}$) which is the difference between
 269 high and low tide volumes or throughput in the channel(s) over an ebb tide (Sheldon
 270 and Alber, 2006). For an implicit timescale of a tidal cycle, V_{TP} represents the volume
 271 change or throughput over the tidal period, T_{TC} .

272

$$T_{TC} = \frac{V_L}{V_{TP}} = \frac{\bar{V}}{\Delta V / T_{TC}} \quad (8)$$

273

274 In the above equation, the overbar represents the integrated mean values of the
275 polynomial curve fit. We assume negligible difference in concentration values at each
276 lagoon entrance at all times.

277

278 **3. Applied theory**

279 **3.1 Measurements and Analysis**

280 Sampling was conducted in surface waters in daylight hours during an ebb tide
281 pilot study on 1 August 2013 (JD 213) and over a complete tidal cycle during spring
282 tide on 20 August 2013 (JD 232) within a 20 m radius of the culvert entrances at Four
283 Mile Bridge and Stanley Embankment (Figure 1). No precipitation occurred during this
284 time. Single-point current velocity measurements were taken in triplicate at 10- or 15-
285 minute intervals at channel inlets during ebb tides throughout July and August using a
286 Braystoke BFM002 miniature current flow meter. Combined half hour moving averages
287 of these measurements were used to validate model estimates (section 3.2). Solar
288 irradiance was determined from hourly moving averages of data supplied by the
289 observatory at Hilbre Island (53°22.980'N, 3°13.680'W) and is used to support
290 evidence of thermal changes in the lagoon.

291 The seawater DIC concentration, partial pressure of CO₂ in seawater ($p\text{CO}_{2W}$)
292 and hence the air-sea CO₂ transfer rate (F_{GAS}), were all computed from temperature,
293 practical salinity, TA, and pH measurements using CO2Calc version 1.2.0 (Robbins et
294 al., 2010). Parameters were determined by setting the seawater pH scale using the
295 Dickson and Millero (1987) re-fit of the Mehrbach et al. (1973) stoichiometric
296 dissociation constants of dissolved CO₂, the stoichiometric dissociation constant of
297 HSO₄⁻ (K_{HSO_4}) in Dickson (1990), the total boron concentration in Lee et al. (2010) and
298 air-sea transfer rate parameters of Wanninkhof (1992). Combined hourly moving
299 averages of wind velocity data provided from meteorological stations at Valley
300 (53°16.980'N, 4°33.780'W, 9 m elevation) and Rhoscolyn (53°14.760'N, 4°34.980'W,
301 13 m elevation) on Anglesey were included to calculate gas transfer velocity (k), in
302 order to estimate the air-sea CO₂ flux also (section 2.2.2). The global average for
303 atmospheric CO₂ concentration (396.7 ppm, NOAA, 2013) was utilized in all
304 calculations of the air-sea $p\text{CO}_2$ gradient necessary for the computation of the air-sea
305 CO₂ transfer rate, as local values are not available nor were in-situ values recorded.

306 Salinity was measured in sub-samples in the laboratory at ambient temperature
307 (18 - 22°C) using a portable conductivity meter (WTW Cond 3110) with a WTW
308 Tetracon 325 probe. TA was determined within four days of collection from
309 refrigerated, unfiltered, un-poisoned seawater samples stored in 500 mL borosilicate
310 bottles with ground-glass stoppers sealed with vacuum grease (Apiezon M). The TA

311 analysis was conducted by potentiometric titration with HCl of sample aliquots of
312 known weight at constant temperature in a jacketed vessel using a Metrohm Titrand
313 888 unit. The automatic burette, pH meter, Pt temperature probe, Ag/AgCl/KCl
314 reference electrode, and glass electrode were calibrated with buffers traceable to SRM
315 from NIST and PTB (Merck, pH 2.00, 4.01, 7.00, 9.00 and 10.00 at 25°C). Daily
316 duplicate potentiometric titrations of CRMs yielded $2227.70 \pm 0.68 \mu\text{mol kg}^{-1}$ for Batch
317 #102 ($n = 19$, certified TA = $2227.46 \pm 0.67 \mu\text{mol kg}^{-1}$) and $2221.22 \pm 1.44 \mu\text{mol kg}^{-1}$
318 for Batch #112 ($n = 6$, certified TA = $2223.26 \pm 0.89 \mu\text{mol kg}^{-1}$). The coefficient of
319 variation as relative standard deviation for TA was better than 0.2%.

320 A combined glass electrode and temperature probe (Inlab, 0.1°C resolution)
321 coupled to a portable Mettler Toledo SG2 (MT+2) pH meter were used for seawater
322 temperature and pH measurements. The Inlab combination electrode was calibrated
323 using the buffers described above in a jacketed vessel at constant temperature every
324 2°C from 5 to 20°C and at 25°C. Linear regression of electrode-buffer potential E (in
325 mV) versus NIST buffer pH yielded the electrode-specific apparent standard potential
326 (E_o) and potentiometric slope as a function of temperature (Figure 4a). The
327 potentiometric slope deviated by 1.2% from ideal electrochemical behavior as
328 expressed by the Nernst slope in the temperature range of 10 to 25°C.

329 The E_o and potentiometric slope temperature functions were used to compute
330 seawater pH on the NIST scale from the in-situ electrode-seawater E and temperature
331 measured at 15-minute intervals by immersing the electrode in the main water mass for
332 a period of no less than 120 s. The MT+2 pH meter offered 1 mV resolution, equivalent
333 to 0.02 pH unit measurement uncertainty. The seawater pH on the seawater scale
334 (pH_{SWS}) was determined from pH_{NIST} as $\text{pH}_{\text{SWS}} = \text{pH}_{\text{NIST}} + \log(f_{\text{H}^+})$, with f_{H^+} equal to the
335 apparent proton activity coefficient determined at the in-situ salinity as a function of
336 temperature by potentiometric titration (outlined above) as described in Gleitz et al.
337 (1995). For this purpose, the Inlab electrode was coupled to the Metrohm titration
338 system, and Inland Sea water was titrated for TA in triplicate every 5°C from 10°C to
339 25°C. The f_{H^+} exhibited a linear temperature dependency at $S = 34.9$ of the seawater
340 sample (Figure 4b).

341

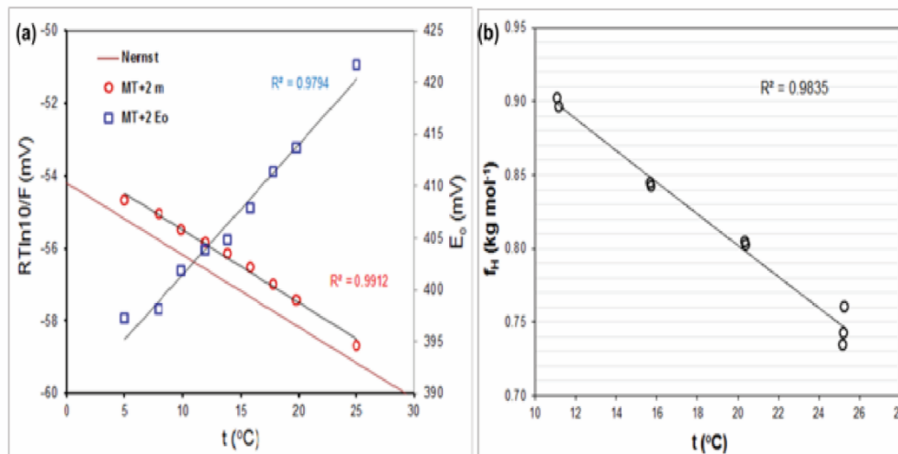


Figure 4. (a) Measured and ideal (Nernst) potentiometric slope ($RT \ln 10 / F$) and apparent standard potential (E_o) as a function of temperature of the Mettler Toledo Inlab combination pH-temperature probe using NIST buffer solutions. (b) Apparent proton activity coefficient (f_{H^+}) as a function of temperature at $S = 34.9$ in seawater. The straight lines through the data represent linear regression fits.

342

343 3.2 Hydrodynamic model validation

344 Thirty-minute moving averages of single point flow measurements during ebb
 345 tide through both channels of the Inland Sea compare well against model outputs
 346 (Figure 5). Mean (± 1 s.d) channel velocities of $1.65 \pm 0.10 \text{ m s}^{-1}$ ($n = 14$), 1.74 ± 0.18
 347 m s^{-1} ($n = 11$), and $1.02 \pm 0.04 \text{ m s}^{-1}$ ($n = 10$) were recorded using the flow meter on 17
 348 July 2013 (JD 198), 19 July 2013 (JD 200), and 1 August 2013 (JD 213), respectively.
 349 Simulated model outputs for the same periods provided $1.37 \pm 0.12 \text{ m s}^{-1}$ ($n = 64$), 1.66
 350 $\pm 0.06 \text{ m s}^{-1}$ ($n = 45$), and $1.05 \pm 0.05 \text{ m s}^{-1}$ ($n = 44$).

351

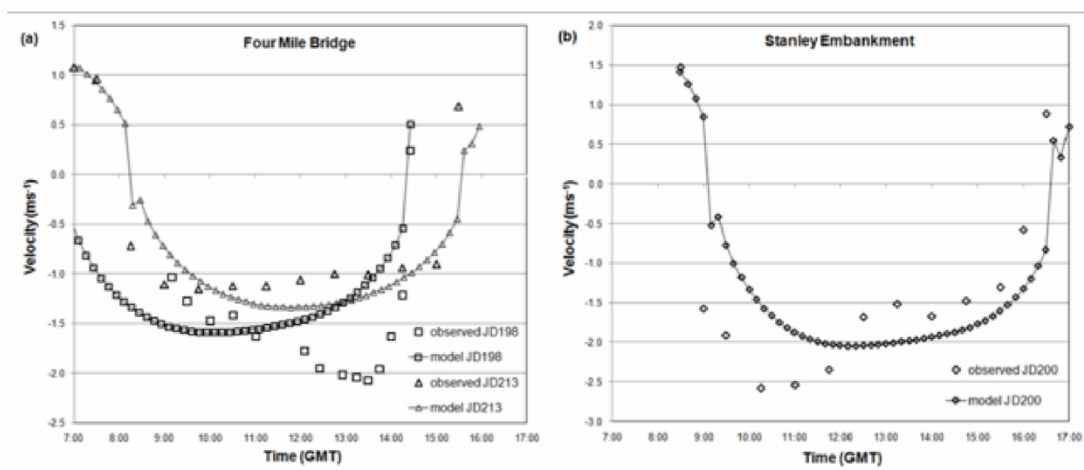


Figure 5. Modelled and observed channel currents. Negative values denote water ebbing away from the lagoon as it empties. Observations were made at culvert entrances to the lagoon at (a) Four Mile Bridge and (b) Stanley Embankment.

352

353 Modelled boundary tidal forcing, expressed as ocean elevation and phase
 354 change at Holyhead (degrees converted to decimal days to provide comparison
 355 continuity) for 1 July 2013 (JD 182) to 31 August 2013 (JD 243) inclusive are compared
 356 to values published by EasyTide, having decimeter resolution (Figure 6). Mean (± 1
 357 s.d) variation in modelled ocean surface elevation above chart datum (ACD) against
 358 published values is 9.5 ± 0.4 cm and the mean variation in phase $1.74^\circ \pm 0.07^\circ$
 359 equivalent to $0.06 \pm 2.4 \times 10^{-3}$ hr ($n = 239$). Field observations of high and low water
 360 times within the Inland Sea are used to validate modelled lagoon phase dynamics
 361 (Table 1). These compare well to model predictions; the mean deviation of the
 362 modelled lagoon phase is $3.06^\circ \pm 2.50^\circ$ or 0.11 ± 0.09 hr ($n = 9$). Tidal range within the
 363 lagoon was also recorded on various days during the study, these observations
 364 deviated from modelled lagoon elevation by 2.0 ± 0.7 cm ($n = 4$). Modelled lagoon
 365 surface area minimum and maximum values of 2.43 km^2 and 6.50 km^2 were estimated
 366 for the period.
 367

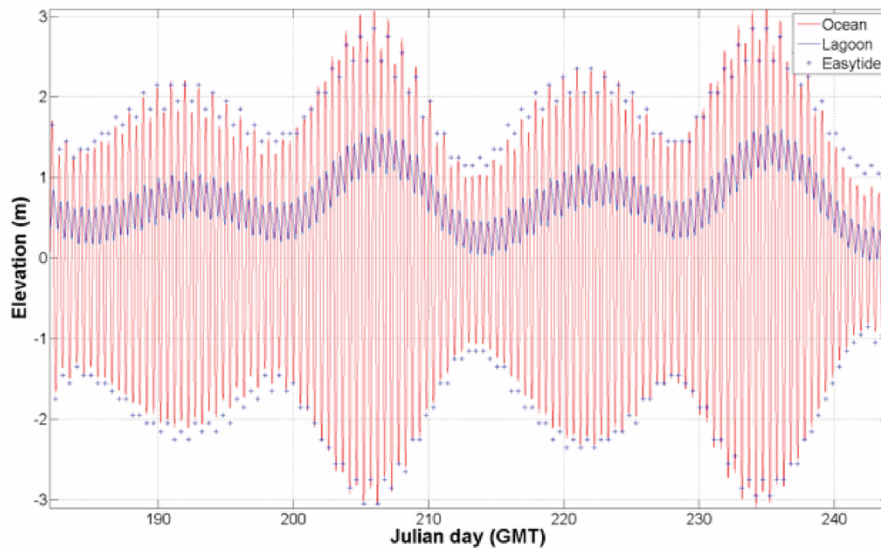


Figure 6. Modelled boundary forcing (red line) based on tidal harmonics at Holyhead compared to published EasyTide data (blue crosses). Simulated lagoon elevation change (blue line) is also plotted.

368
 369
 370
 371

Table 1 Observations of lagoon high and low water times used to validate modelled lagoon tidal phase and range.

Lagoon tidal phase (hh:mm GMT)		
observed	model	error
JD192 09:37	09:45	+00:08
JD198 14:20	14:12	-00:08
JD200 08:47	08:49	+00:02
JD200 16:15	16:26	+00:11
JD213 07:56	07:59	+00:03
JD213 15:19	15:20	+00:01

JD232 06:57	07:02	+00:05
JD232 11:25	11:23	-00:02
JD232 18:52	19:09	+00:17

Lagoon tidal range (m)

JD200 0.45	0.46	+0.01
JD213 0.42	0.43	+0.01
JD232 0.49	0.47	-0.02
JD232 0.46	0.50	+0.04

372

373 **4. Results**

374 Mass balance of DIC is controlled by a combination of physical and biological
375 processes. These include temperature change, water mixing, photosynthetic
376 production of organic material, respiration of marine biota, calcium carbonate
377 precipitation and dissolution, and air-sea transfer of CO₂ across the surface boundary
378 layer. Photosynthesis, CaCO₃ precipitation and CO₂ evasion all consume DIC, while
379 respiration, CaCO₃ dissolution and CO₂ transfer from atmosphere recycle carbon back
380 into the DIC pool from the organic, mineral and gaseous phases, respectively
381 (Papadimitriou et al., 2012). An imbalance, therefore, in the sinks and sources of DIC
382 will result in a net change in the DIC concentration in an aquatic system.

383 During these processes, the marine CO₂ system will re-equilibrate, with
384 consequent changes in parameters such as pH and the $p\text{CO}_{2W}$ of the system. The
385 change in DIC concentrations derived from the empirical observations in this study are
386 considered to be the result of influence from some, or all, of the processes of gas
387 exchange, advection and net ecosystem productivity, leading to a net deficit or excess
388 in the balance between fluxes entering and leaving the lagoon. By capturing the carbon
389 exchange rate at ecosystem boundaries, overall assessment of the net balance
390 between these processes is achieved. Our resultant analysis indicates whether the
391 ecosystem acts to balance the carbon budget as a net sink or source during the study
392 period.

393

394 **4.1 Lagoon system**

395 Changes in lagoon water parameters were observed from 08.00 to 19.30 BST,
396 during a complete spring tidal cycle. The mean lagoon water residence time is
397 estimated at 39 ± 6 hr calculated from simulated model channel throughput values
398 (Table 2). Seawater temperature increased linearly from 16.6°C to 19.8°C over the
399 course of the day, reaching a plateau during mid-afternoon while salinity remained
400 relatively constant at 34.01 ± 0.02 (± 1 s.d, $n = 24$). During the flood period, the pH_{sws}
401 varied between 8.05 and 8.13, while during the ebb tide it increased systematically
402 from 8.05 to 8.26. Total alkalinity initially decreased during flood tide from 2329 μmol
403 kg^{-1} to 2300 $\mu\text{mol kg}^{-1}$ and remained relatively constant for most of the ebb tide, with a

404 small step change of $\sim 10 \mu\text{mol kg}^{-1}$ toward the end of the study period. The calculated
 405 DIC and $p\text{CO}_{2W}$ exhibited similar behaviour with sinusoidal fluctuations. During the
 406 flood tide, the DIC exhibited a short initial increase followed by a sustained systematic
 407 decrease from 2092 to 1937 $\mu\text{mol kg}^{-1}$. Over the same period, the $p\text{CO}_{2W}$ fluctuated
 408 between 312 μatm and 394 μatm during flood and exhibited a systematic decrease
 409 from 330 μatm to 220 μatm during ebb (Figures 7 and 8; Table 3).

410 The $p\text{CO}_{2W}$ indicates that, throughout the study period, CO_2 levels in the lagoon
 411 were conducive to transfer of CO_2 from the atmosphere to seawater. Wind velocity
 412 increased over the course of the day from 1.6 m s^{-1} at the start of the study to almost 5
 413 m s^{-1} by the end (Figure 8). The F_{GAS} calculations were estimated to be negative
 414 throughout the study period (Figure 9), indicating again that the air-sea exchange of
 415 CO_2 occurred from atmosphere to seawater. There was an increase from a minimum
 416 air-sea flux of $-0.002 \text{ mmol C m}^{-2} \text{ hr}^{-1}$ to a maximum of $-0.38 \text{ mmol C m}^{-2} \text{ hr}^{-1}$, with a
 417 mean ($\pm 1 \text{ s.d.}$) $F_{\text{GAS}} = -0.13 \pm 0.26 \text{ mmol m}^{-2} \text{ hr}^{-1}$. The mean NEP rate for this tidal
 418 period is estimated at $3.0 \pm 0.4 \text{ mmol C m}^{-2} \text{ hr}^{-1}$ (Table 3), with F_{GAS} equivalent to 4.3%
 419 of NEP DIC provision.

420

421 **Table 2** Calculated water residence time based on cumulative modeled channel flow data over
 422 the mean ebb and flood period during sampling.

423

	Flood ($\text{m}^3 \text{ hr}^{-1}$)	Ebb ($\text{m}^3 \text{ hr}^{-1}$)	Water Residence Time (hr)
Min	3032258	1098513	33.4
Max	3057142	823390	45.0
Mean Period (hr)	4.5	7.6	

424

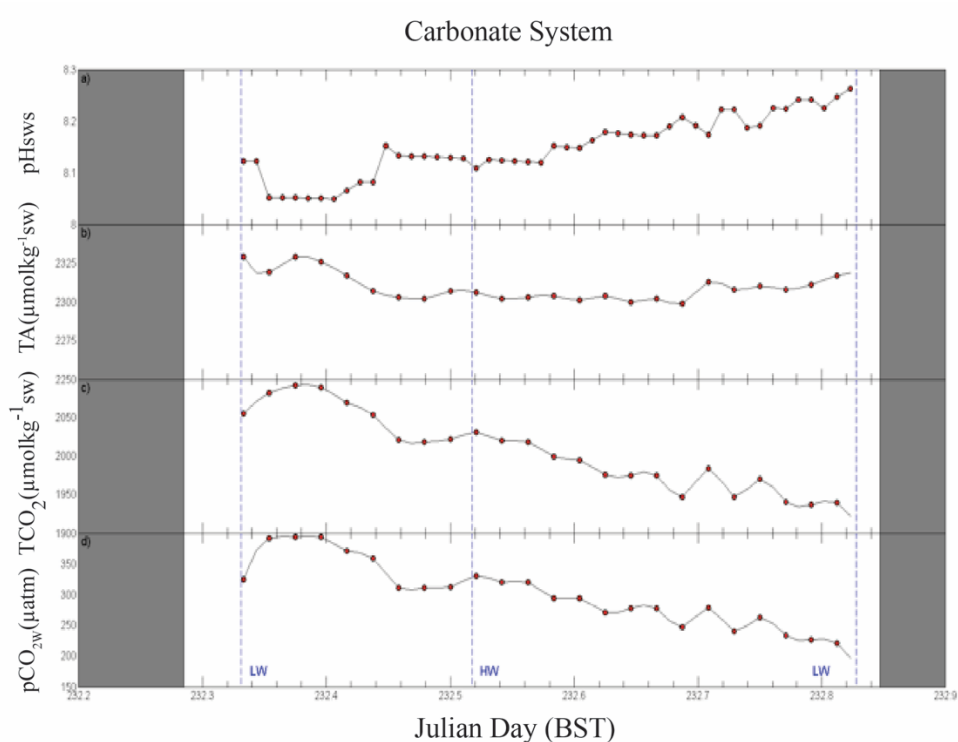


Figure 7. Lagoon carbonate system parameters of (a) pH (b) TA (c) DIC and (d) $p\text{CO}_2$ on JD 232 (solid markers). DIC and $p\text{CO}_2$ are derived from CO2Calc estimates of in-situ pH and TA observations. High and low water (blue lines) and non-daylight hours (grey areas) are also indicated.

425

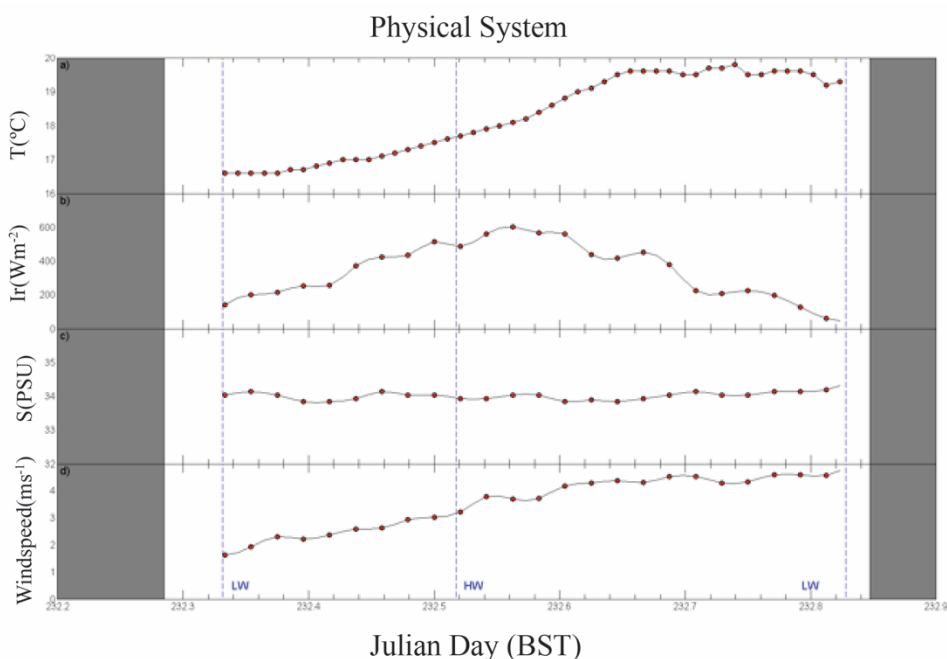


Figure 8. Lagoon physical parameters of (a) water temperature (b) surface solar irradiance (c) salinity (d) and surface wind speed observed on JD 232. High and low water (blue lines) and non-daylight hours (grey areas) are also indicated.

426

427 **Table 3** Measured seawater salinity, temperature, pH and TA along with calculated DIC, $p\text{CO}_2$,
 428 and air-sea CO_2 exchange rate (F_{GAS}) in the Inland Sea. The NEP value is the overall estimated
 429 daytime average. A net carbon sink is inferred from a positive NEP value and a negative F_{GAS}
 430 indicates a net transfer of CO_2 from the atmosphere to seawater. The mean water residence

431 time was derived from a validated 1-D MATLAB model of boundary volumetric flow, while DIC
 432 ($\pm 8 \mu\text{mol kg}^{-1}$) and $p\text{CO}_2$ ($\pm 20 \mu\text{atm}$) were derived from CO2Calc.
 433

	NEP				Mean Water Residence Time									
	(mmol C m⁻² hr⁻¹)				(hr)									
	3.0 ± 0.4				39 ± 6									
Time (BST)	Salinity		Temp (°C)		pH_{sws}		TA		DIC		pCO₂		F_{Gas}	
							($\mu\text{mol kg}^{-1}$)	($\mu\text{mol kg}^{-1}$)	(μatm)	(μatm)	(μatm)	(μatm)	(mmol C m ⁻² hr ⁻¹)	(mmol C m ⁻² hr ⁻¹)
	JD213	JD232	JD213	JD232	JD213	JD232	JD213	JD232	JD213	JD232	JD213	JD232	JD213	JD232
08:00	33.3	34.0	17.5	16.6	8.04	8.12	2323	2329	2089	2055	406	325	0.022	-0.020
08:30	33.4	34.1	17.5	16.6	8.04	8.05	2323	2319	2089	2082	405	391	0.020	-0.002
09:00	33.4	34.0	17.5	16.6	8.04	8.05	2326	2329	2092	2092	406	394	0.016	-0.002
09:30	33.5	33.8	17.5	16.7	8.04	8.05	2325	2326	2090	2090	405	394	0.017	-0.002
10:00	33.4	33.8	17.5	16.9	8.04	8.07	2330	2317	2095	2070	407	371	0.022	-0.015
10:30	33.0	33.9	17.6	17.0	8.04	8.08	2333	2307	2100	2054	409	359	0.020	-0.026
11:00	33.3	34.1	17.8	17.1	8.06	8.13	2333	2303	2082	2020	385	312	-0.017	-0.061
11:30	33.3	34.0	18.0	17.3	8.09	8.13	2331	2302	2067	2019	355	312	-0.054	-0.076
12:00	33.3	34.0	18.3	17.5	8.08	8.13	2327	2307	2064	2021	364	312	-0.040	-0.080
12:30	33.5	33.9	18.7	17.7	8.08	8.11	2316	2306	2051	2031	362	330	-0.044	-0.072
13:00	33.6	33.9	19.1	17.9	8.11	8.12	2308	2302	2023	2020	331	321	-0.083	-0.113
13:30	33.6	34.0	19.6	18.1	8.12	8.12	2309	2303	2014	2018	322	320	-0.081	-0.109
14:00	33.6	34.0	19.9	18.4	8.12	8.15	2310	2304	2012	1999	322	294	-0.086	-0.147
14:30	33.6	33.8	20.2	18.8	8.13	8.15	2314	2301	2007	1994	313	294	-0.093	-0.185
15:00	33.4	33.9	20.5	19.1	8.16	8.18	2317	2304	1988	1976	288	270	-0.121	-0.242
15:30	33.6	33.8	20.5	19.5	8.16	8.17	2319	2300	1991	1975	288	277	-0.090	-0.236
16:00	33.6	33.9	20.7	19.6	8.21	8.17	2322	2302	1955	1975	249	277	-0.166	-0.229
16:30	33.7	34.0	20.3	19.6	8.18	8.21	2317	2299	1973	1946	271	246	-0.143	-0.318
17:00		34.1		19.5		8.17		2313		1984		278		-0.251
17:30		34.0		19.7		8.22		2308		1947		240		-0.298
18:00		34.0		19.5		8.19		2310		1970		263		-0.260
18:30		34.1		19.6		8.23		2308		1941		233		-0.357
19:00		34.1		19.6		8.24		2311		1937		227		-0.369
19:30		34.2		19.2		8.25		2317		1939		221		-0.380

434

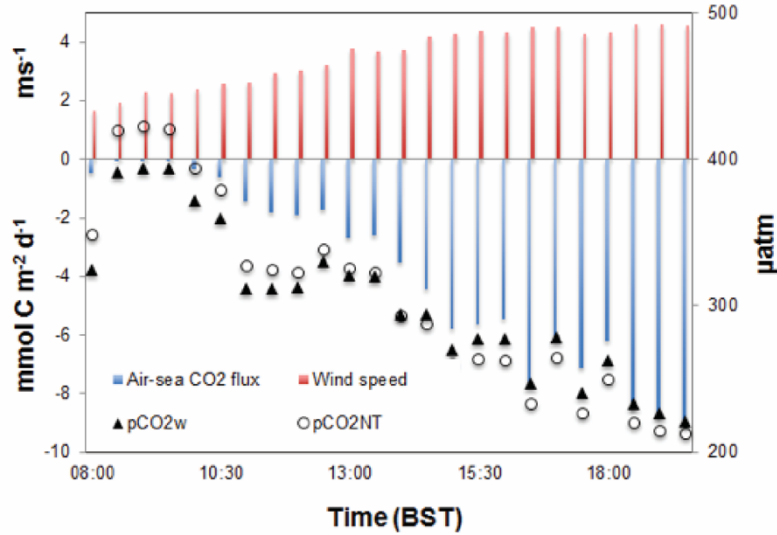


Figure 9. Air-sea CO₂ exchange, wind velocity, $p\text{CO}_{2W}$ and temperature normalized partial pressure of CO₂, $p\text{CO}_{2,NT}$ for the study period on JD 232. Outgassing inferred from $p\text{CO}_{2,NT}$ values early in the study period is prevented by low water temperature that increases gas solubility and lowers $p\text{CO}_{2W}$ preventing transfer of CO₂ from lagoon to atmosphere.

435

436 5. Discussion

437 5.1 Thermal effects

438 Temperature change affects the solubility of CO₂ in water, whereby an increase
 439 in temperature by 1°C causes approximately 4% $p\text{CO}_{2W}$ increase as the dissolved gas
 440 dissociates (Gazeau et al., 2005; Jiang et al., 2011; De Carlo et al., 2013). Using
 441 CO2Calc to assess the maximum possible change of $p\text{CO}_{2W}$ ($\Delta p\text{CO}_{2,T}$) from the
 442 temperature variation observed over the full tidal cycle on JD232 by fixing DIC and TA
 443 values at the lowest observed diel temperature and allowing pH to vary with inputs of
 444 minimum and maximum recorded temperature, we found that $\Delta p\text{CO}_{2,T} = 46 \mu\text{atm}$. This
 445 is the maximum extent to which the temperature change within the lagoon can affect
 446 the $p\text{CO}_{2W}$ of the system ($p\text{CO}_{2,T}$) during the study period. This value was confirmed by
 447 isolating the thermally forced $p\text{CO}_{2W}$ changes to reveal only the change due to $p\text{CO}_{2,T}$
 448 using the approach of Takahashi et al. (1993).

449

$$p\text{CO}_{2,T} = p\text{CO}_{2,\text{mean}} \times e^{0.0423 \times (T_{\text{obs}} - T_{\text{mean}})} \quad (9)$$

450

451 Here $p\text{CO}_{2,T}$ and $p\text{CO}_{2,\text{mean}}$ are the $p\text{CO}_{2W}$ values from thermal forcing alone and the in-
 452 situ average, respectively, while T_{mean} and T_{obs} are the in-situ mean and observed
 453 water temperature, respectively. This thermally isolated change reveals a similar 40
 454 μatm change for the 3.2°C temperature increase observed in the lagoon water,
 455 resulting in only a 3.8% difference in value.

456 A maximum diel range in $p\text{CO}_{2\text{W}}$ of approximately 172 μatm as observed on JD
457 232 (Figure 9) can be attributed to a combination of the remaining physical and
458 biogeochemical processes within the lagoon, which have over three times the influence
459 that temperature effects alone can explain. We used a similar approach in order to
460 isolate the influences of the non-thermal processes of mixing, gas exchange and
461 biological activity from the temperature effect on $p\text{CO}_{2\text{W}}$ by normalizing to the mean
462 temperature during empirical observations ($p\text{CO}_{2,\text{NT}}$) using the following formula:
463

$$p\text{CO}_{2,\text{NT}} = p\text{CO}_{2,\text{Tobs}} \times e^{0.0423 \times (T_{\text{mean}} - T_{\text{obs}})} \quad (10)$$

464
465 where $p\text{CO}_{2,\text{NT}}$ and $p\text{CO}_{2,\text{Tobs}}$ are the $p\text{CO}_{2\text{W}}$ values from temperature normalized and
466 actual observation calculations, respectively. The normalized values along with $p\text{CO}_{2\text{W}}$
467 can be compared to reveal the time-based influence of temperature on the system.

468 The relative importance of thermal contribution over the course of the study
469 period is highlighted by the lower temperatures in the lagoon at the start of the study
470 due to low solar irradiance and the influence of incoming seawater. These factors
471 promote greater solubility of CO_2 and act to prevent the system from outgassing to
472 atmosphere during this time. As the day progresses and the absorbed radiant energy
473 peaks, the thermal contribution predictably acts to increase $p\text{CO}_{2\text{W}}$. Given an assumed
474 constant $p\text{CO}_{2\text{A}}$ (396.7 ppm, NOAA, 2013), the air-sea flux drives CO_2 into the water
475 column due to the increasing $p\text{CO}_2$ gradient, aided by an increase in wind velocity as
476 the study period progressed, thus promoting aquatic CO_2 uptake (Takahashi et al.,
477 2002). It should also be noted that the influence of processes acting to reduce $p\text{CO}_{2\text{W}}$
478 appear to have greater impact in the lagoon than that of air-sea exchange influenced
479 by wind speed (Figure 9).

480 Using CO2Calc (section 3.1) we compute pH_{25} from the recorded salinity, TA
481 and DIC values (Table 3) and compare this with the in-situ pH data. As temperature
482 has a significant impact on this parameter, the temperature corrected value highlights
483 the biological influence in the signal. The corrected 25°C value is warmer than in-situ
484 measurements, therefore we expect to see lower pH_{25} values. A clear reduction in the
485 signal difference over time can be seen in Figure 10 as the lagoon system warms. The
486 difference in the two pH values has a scale corrected range from 88.0% (08.30 to
487 09.00) to 93.4% (17.30) that can be attributed to biological activity alone.

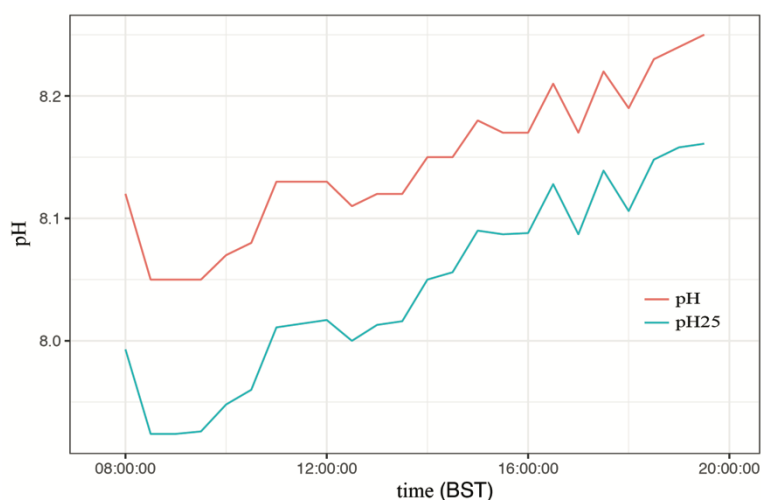


Figure 10. The pH₂₅ was computed using CO2SYS from measured salinity, TA, and DIC values (Table 3), using a constant temperature of 25°C.

488

489 5.2 Biogeochemical effects

490 Using the stoichiometry of potential contributing biogeochemical processes that
 491 could affect the CO₂ system of the lagoon, the fractional contribution of each to the TA-
 492 DIC mass balance can be assessed. This is achieved by examining the distribution of
 493 salinity-normalized values of lagoon TA against DIC concentration relative to the
 494 equivalent incoming seawater concentration from outside the basin. Photosynthesis will
 495 cause a slight increase in TA due to nutrient uptake and will reduce the DIC
 496 concentration due to its uptake by primary producers within the system, whereas
 497 respiration will have the opposite effect. Both processes result in a low ratio of TA to
 498 DIC concentration change, with $\Delta A_T : \Delta C_T = -0.16$ (Lazar and Loya, 1991; Wolf-Gladrow
 499 et al., 2007). The ratio of TA to DIC concentration change during calcification and
 500 CaCO₃ dissolution is 2, while for benthic anaerobic respiration via sulphate reduction
 501 with sulphide accumulation in sediment pore waters, $\Delta A_T : \Delta C_T = 1$ (Wang & Cai 2004;
 502 Wolf-Gladrow et al., 2007; Soetaert et al., 2007; Zhai et al., 2017).

503 The dominance of each of these processes to the biogeochemistry of the
 504 lagoon depends on a number of factors and could be overridden by external forces,
 505 such as freshwater input, lagoon stratification, and water residence time (Gupta et al.,
 506 2008; Kone et al., 2009; Muduli et al., 2012; Zhai et al., 2017). Their magnitude and
 507 seasonal variability will affect the biogeochemistry of the lagoon and the net air-sea
 508 CO₂ exchange. The trend in the current salinity-normalized TA versus DIC data over
 509 the study period suggests that the carbonate system in the lagoon at full insolation was
 510 influenced by photosynthesis and CO₂ transfer from the atmosphere (Figure 11). The
 511 sustained increase of pH with temperature and stable TA throughout the heightened
 512 solar period, combined with an increased air-sea flux gradient suggests that maximum
 513 utilization of CO₂ occurs within the lagoon. Some moderate fluctuation in the normally
 514 conservative TA parameter (Figure 7) suggests that it was affected somehow during

515 the study, but no water mass mixing occurs and CaCO_3 precipitation-dissolution
 516 appears to be negligible as a $\Delta A_T : \Delta C_T = 2$ in the salinity-normalized values would be
 517 expected (Figure 11).
 518

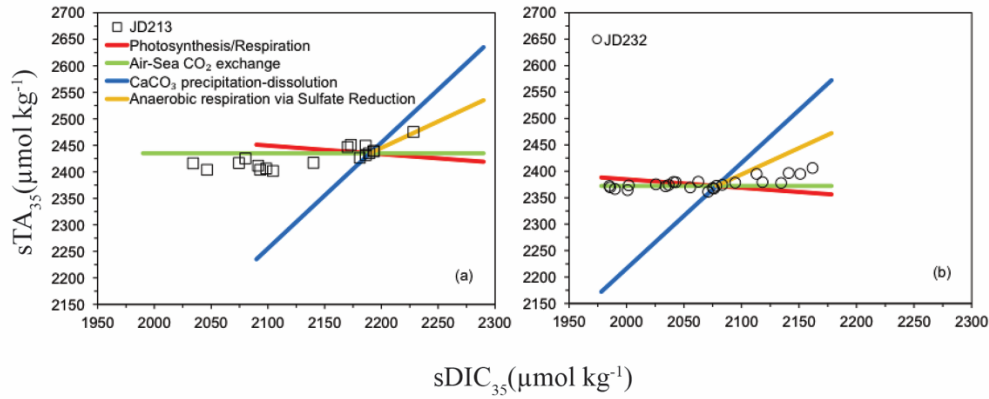


Figure 11. TA versus DIC concentrations in lagoon water observed during (a) JD 213 and (b) JD 232 normalized to $S = 35$, plotted relative to the inflowing seawater on each day. This is considered to be the baseline matrix altered by the physical-biogeochemical processes in the lagoon. The solid, colour coded lines indicate data distribution when individual physical-biogeochemical reactions dominate the carbonate system.

519

520 In studies of deeper coastal environments where only pelagic communities
 521 dominate, temperature drives short-term changes in the carbonate system (Dai et al.,
 522 2009). This study suggests that, in agreement with Jiang et al. (2011), within shallow
 523 nearshore systems, alterations driven by autotrophic benthic organisms may contribute
 524 most to ecosystem change.

525

526 5.3 Tidal influence

527 Overlaying the eularian carbonate system analyses during sampling periods
 528 highlights the tidal influence on the biological signal (Figure 12). The ebbing tide
 529 sampled on JD 213 exhibits a maximum lagoon DIC concentration of around 2090
 530 $\mu\text{mol kg}^{-1}$ at the start of observations (09.30) likely due to the overnight predominance
 531 of CR. The DIC concentration systematically decreases from that point throughout the
 532 day to around 1950 $\mu\text{mol kg}^{-1}$ with an approximate linear trend of $-20 \mu\text{mol kg}^{-1} \text{ hr}^{-1}$
 533 driven by autotrophic activity linked with increasing solar irradiance, which had a mean
 534 value of $580 \pm 42 \text{ W m}^{-2}$ ($\pm 1\text{s.d.}$, $n = 18$) over the period.

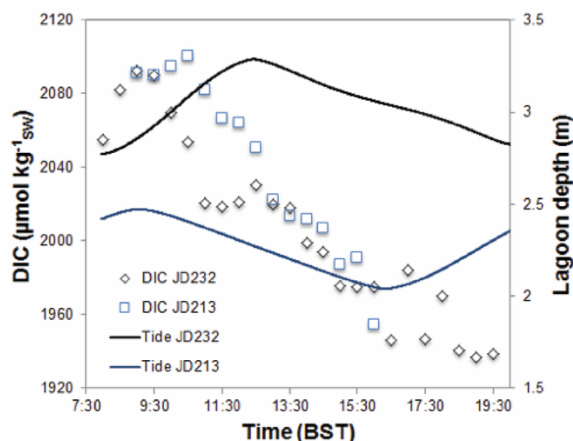


Figure 12. Lagoon tidal regime and observed inlet DIC concentration for both JD213 and JD232. A distinct pattern of diurnal biological production during the semi-diurnal tidal cycle fluctuation is present, indicating nutrient availability from tidal ebb and flood and daytime biology utilisation.

535

536 By comparison, during JD 232 when sampling started (08.00) on a flood tide,
 537 the DIC concentration within the lagoon initially increased from 2050 $\mu\text{mol kg}^{-1}$ to 2090
 538 $\mu\text{mol kg}^{-1}$ due to a proportion of lagoon water that had earlier vacated the lagoon being
 539 forced back by the tide. Mixing of water carried back into the lagoon initially attenuates
 540 any biologically driven DIC concentration decrease. Net DIC loss becomes apparent
 541 after 09.30 when a sharp concentration drop was observed. The overall linear trend is
 542 approximately $-13 \mu\text{mol kg}^{-1} \text{hr}^{-1}$ for a mean solar irradiance of $334 \pm 35 \text{ W m}^{-2}$ ($\pm 1 \text{ s.d.}$,
 543 $n = 25$). As the sampling occurred during daylight hours, primary production appears to
 544 be the driver of DIC concentration change over time at this site. In contrast, community
 545 respiration would be expected to dominate at night (Frankignoulle and Bouquegneau,
 546 1990) and during winter periods (Delille, Borges and Delille, 2009).

547

548 **5.4 Diel NEP rate**

549 The contribution of atmospheric carbon via CO_2 transfer from atmosphere to the
 550 lagoon during the sampling period was estimated to be 4.3% of NEP. Conceivably, this
 551 is as a direct result of the photosynthetic uptake in the Inland Sea. Jiang et al. (2011)
 552 and Muduli et al. (2013) report similar findings, with CO_2 transfer from the atmosphere
 553 playing a significant role in the latter study. In this study we determined a positive NEP
 554 of $3.0 \pm 0.4 \text{ mmol C m}^{-2} \text{ hr}^{-1}$, which indicates a net carbon sink due to primary
 555 production during daytime. This is the average ecosystem metabolism during the
 556 photic semi-diurnal period of study (12.12 hr). Therefore, approximately 96% of the
 557 daytime carbon NEP budget in the lagoon was supported by DIC availability from
 558 advected nutrients while the remainder came from surface interface atmospheric CO_2

559 transfer. The estimated time-integrated metabolic rate for the 13.5 hr total daylight
560 period is then equivalent to 40.5 ± 5.4 mmol C m⁻².

561 We lack site-specific information on CR, however, Hopkinson and Smith (2005)
562 report pelagic respiration rates in shallow inshore waters of between 58 and 114 mmol
563 C m⁻² d⁻¹. Thus, assuming an overnight CR range of 2.42 – 4.75 mmol C m⁻² hr⁻¹ NEP
564 estimates during our study period would yield values between 15.23 and -9.24 mmol C
565 m⁻² d⁻¹. Whereas using a CR value of 279 ± 184 mmol O₂ m⁻² d⁻¹ ($n = 7$) measured in *Z.*
566 *noltii* meadows in the Thau lagoon, France, and a photosynthetic quotient of 1 (Duarte
567 et al., 2010), a time-integrated CR of 122 ± 81 mmol C m⁻² can be calculated over the
568 10.5 hr respiration-dominated night-time period. This then suggests a diel NEP rate of
569 approximately -82 ± 81 mmol C m⁻² d⁻¹ for our study site; the former range of estimates
570 being more consistent with the median NEP value of 20.6 mmol C m⁻² d⁻¹ reported in
571 seagrass ecosystem studies (Johnson et al., 2017).

572 Tokoro et al. (2014) presented global seagrass ecosystem NEP rates of 27 ± 6
573 mmol C m⁻² d⁻¹ converted from oxygen-based units. NEP estimates and errors may
574 vary dependent upon applied method and location. For example, Gazeau et al. (2005)
575 found that measured NEP rates fluctuated between 7 ± 1 mmol C m⁻² d⁻¹ and 41 ± 3
576 mmol C m⁻² d⁻¹, with a mean of 22 ± 12 mmol C m⁻² d⁻¹. Estimates of water residence
577 times, which are difficult to quantify in open embayment's, contributed most to
578 uncertainty. Ribas-Ribas et al. (2011) found NEP values between 10 and 60 mmol C m⁻²
579 d⁻¹ neglecting the influence of water residence time. Other studies have assessed
580 whether net autotrophic or heterotrophic behavior dominates in coastal systems based
581 on longer studies of NEP, estimated from rates of GPP and CR, with GPP known to
582 vary inter-annually by as much as 35% and NEP by 87% (Champenois and Borges,
583 2012).

584 The intertidal beds of the Inland Sea are colonized by the seagrass *Zostera*
585 *noltii*, which contribute to primary production in the study area. Papadimitriou et al.
586 (2006) estimated an increase in the above-ground seagrass biomass equivalent to 18
587 – 27 mmol C m⁻² d⁻¹ and in the below-ground biomass (roots and rhizomes) equivalent
588 to 22 – 28 mmol C m⁻² d⁻¹ during growth periods in spring and summer. Duarte et al.
589 (2005) reported on GPP, CR, and NEP for seagrass species and found that, in general,
590 seagrass meadows with $GPP \geq 180$ mmol C m⁻² d⁻¹ were net autotrophic. Specifically,
591 for *Z. noltii*, ~66% of the meadows included in the Duarte et al. (2010) study had GPP
592 values of this magnitude, attesting to the potential for carbon sequestration for this
593 species of seagrass. Based on the limited daytime NEP data and assumed night-time
594 CR of Duarte et al. (2010), the seagrass community in our study site may be net
595 heterotrophic on an annual time scale but more detailed investigation is required to
596 validate this indication. Thus, future modelling of lagoon systems would benefit from

597 diurnal and seasonal sampling of the CO₂ system to obtain annual estimates of net
598 carbon gain or loss to the atmosphere and to the adjacent Irish Sea waters.

599

600 **5.5 Residence time**

601 The box model approach utilized here allows us to quantify the input and output
602 of CO₂ in the system from both advective lateral fluxes and surface transfer regimes,
603 which is crucial in shallow nearshore ecosystems. However, it requires the ability to
604 accurately predict water flow through the channels, because large uncertainties are
605 introduced into calculations over short time scales (Borges et al., 2008). By considering
606 an integrated approach over a tidal period, the uncertainty is somewhat attenuated.
607 The integrated mean used to derive mass balance calculations are based on
608 polynomial fits of the plotted observational data, with 95% confidence intervals of the
609 standard deviation of the slope used to constrain NEP calculations.

610 Based on simplified unidirectional, unforced and hydrostatically balanced
611 channel flow calculations ($0.5 u^2 = -g d\eta/dx$) the contribution to error from uncertainty in
612 harmonic boundary forcing in the MATLAB simulations causes a maximum elevation
613 uncertainty of approximately 10 cm. This yields a maximum potential flow uncertainty
614 of around 0.14 m s⁻¹ in a channel of 100 m length (this error reduces for longer
615 channels). However, validation data resolution was of the same order of magnitude,
616 therefore this was ignored for NEP error estimate. The largest contribution to
617 uncertainty for this study came from the estimated lagoon phase error of 0.11 ± 0.09 hr
618 ($n = 9$). Assuming an average flow through the channel over the error phase period of
619 0.5 m s⁻¹ (i.e. around slack water), a maximum difference in ΔF_{MIX} of approximately 0.15
620 mmol C m⁻² is possible. Therefore, greatest uncertainty is derived from the change in
621 water residence time with phase shift. This results in an increase in the cumulative
622 error estimation from ± 0.03 mmol C m⁻² hr⁻¹ to ± 0.4 mmol C m⁻² hr⁻¹ for a calculated
623 difference in mean residence time of approximately 6 hours.

624 Based on a fixed tidal period and using the methods of this study, water
625 residence time will increase if mean lagoon capacity increases or if the change in
626 channel volumetric flow decreases (effectively a decrease in tidal range). An increase
627 in residence time subsequently reduces NEP as the nutrients within the system take
628 longer to be replenished and may result in a loss of seagrass habitat (Orfila et al.,
629 2005). Delhez et al. (2014) report that the total time spent within the control domain
630 may be significantly underestimated in oscillating flow regimes using the approach
631 presented. It should be noted that calculation of residence time based on eq (6) utilizes
632 the simple assumption that all of the water is exchanged through the channel, when in
633 reality some of the water exiting or entering the lagoon returns immediately. A better
634 approach may be to consider the fractional return of some of the water to avoid

635 overestimation of NEP (Sheldon and Alber, 2006; Rynne et al., 2016). Future work
636 should focus on constraining the parameters critical to estimating the time taken for
637 water to be replenished within the lagoon. Increased understanding of the lagoon
638 bathymetry, channel dimensions and substrate type would all conceivably contribute to
639 a reduction in modelled phase error.

640

641 **6. Conclusion**

642 Restricted lagoons such as the Inland Sea offer the ability to examine the
643 variation in NEP from DIC utilization and water residence period due to the nature of
644 their water exchange regimes. Increased high-resolution temporal monitoring using
645 autonomous techniques may be beneficial, as would constraining spatial distribution of
646 carbonate system concentrations. It has been shown that the overall net carbon
647 productivity of the Inland Sea ecosystem can be assessed over a complete tidal period
648 by conducting measurements of carbonate system parameters from water advected
649 through the channels, in combination with post observation, bulk parameterization
650 analysis. Development of methods should include autonomous measurements,
651 improved geophysical evaluation, enhanced validation and numerical hydrodynamic
652 modelling of boundary exchange, in order to further constrain estimates. Extrapolation
653 of calculated values for increased spatial and temporal assessment should also be a
654 future objective.

655 The overall net autotrophic balance of the seagrass containing system studied
656 suggests a potential sink for inorganic carbon during summer periods. An estimated
657 NEP of 40.5 ± 5.4 mmol C m⁻² during the 13.5 hr daytime study period is equivalent to
658 a diel range of between 15.23 and -9.24 mmol C m⁻² d⁻¹ based on assumptions using
659 reported shallow water pelagic respiration rates. However, it is crucial to include
660 measurements of actual overnight respiration rate during studies, as a potential source
661 of inorganic carbon is calculated (-82 ± 81 mmol C m⁻² d⁻¹) when literature values for
662 *Zostera noltii* meadows based on O₂ utilization is assumed. Furthermore, the former
663 approach suggests that approximately 4% of DIC is provided by CO₂ transfer from
664 atmosphere to ocean during the study period. Similar methodology may provide an
665 opportunity to assess the atmospheric carbon sequestration potential of planned
666 nearshore lagoon constructions. From the MRE perspective, there exists the potential
667 of enhancing the financial feasibility of tidal range lagoon energy schemes through
668 consideration of carbon offsetting. In particular when such structures are designed to
669 accommodate colonies of productive autotrophic flora.

670

671 **Acknowledgements**

672 With grateful thanks to Ben Butler and Charlotte Angove for the time, input, and
673 support, they provided during fieldwork and in the laboratory for the duration of this
674 project. The suggestion of using Hilbre Island weather station observatory data for
675 solar irradiance values was kindly made by Madihah Jafar-Sidik and access granted by
676 the Coastal Observatory at Liverpool bay (www.cobs.ac.uk). Meteorological information
677 was accessed at weather underground (www.wunderground.com).

678

679 **References**

680 Auby I, and Labourg P J (1996) Seasonal Dynamics of *Zostera noltii* Hornem in the Bay of
681 Arcachon (France). *Journal of Sea Research* 35, 4: 269-277.

682

683 Barnes R S K (1989) The Coastal Lagoons of Britain: An Overview and Conservation
684 Appraisal. *Biological Conservation*: 295-313.

685

686 Barron C, Duarte C M, Frankignoulle M, and Borges A V (2006) Organic carbon metabolism
687 and carbonate dynamics in a Mediterranean Seagrass (*Posidonia oceanica*) meadow.
688 *Estuaries and Coasts* 29: 417–426.

689

690 Bauer J E, Cai W J, Raymond P A, Bianchi T S, Hopkinson C S, and Regnier P A G (2013)
691 The changing carbon cycle of the coastal ocean. *Nature* 504, 7478: 61-70.

692

693 Borges A V, Delille B, and Frankignoulle M (2005) Budgeting sinks and sources of CO₂ in
694 the coastal ocean: Diversity of ecosystems counts. *Geophysical Research Letters* 32: 1-4.

695

696 Borges A V, Ruddick K, Schiettecatte L S, and Delille B (2008) Net ecosystem production
697 and carbon dioxide fluxes in the Scheldt estuarine plume. *BMC Ecology* 8, 15: 1-10.

698

699 Champenois W, and Borges A V (2012) Seasonal and interannual variations of community
700 metabolism rates of a *Posidonia oceanica* seagrass meadow. *Limnology and*
701 *Oceanography* 57, 1: 347–361.

702

703 Dai M, Lu Z, Zhai W, Chen B, Cao Z, Zhou K, Cai W J, and Chen C T A (2009) Diurnal
704 variations of surface seawater pCO₂ in contrasting coastal environments. *Limnology and*
705 *Oceanography* 54: 735-745.

706

707 De Carlo E H, Mousseau L, Passafiume O, Drupp P S, and Gattuso J P (2013) Carbonate
708 Chemistry and Air-Sea CO₂ Flux in a NW Mediterranean Bay Over a Four-Year Period:
709 2007-2011. *Aquatica Geochemica* 19: 399-442.

710

711 Delhez E J M, de Brye B, de Brauwere A, and Deleersnijder E (2014) Residence time vs
712 influence time. *Journal of Marine Systems* 132: 185-195.
713 <http://dx.doi.org/10.1016/j.jmarsys.2013.12.005>
714

715 Delille B, Borges A V and Delille D (2009) Influence of giant kelp beds (*Macrocystis pyrifera*)
716 on diel cycles of $p\text{CO}_2$ and DIC in the Sub-Antarctic coastal area. *Estuarine, Coastal and*
717 *Shelf Science* 81: 114-122.
718

719 Dickson A G, and Millero F J (1987) A comparison of the equilibrium constants for the
720 dissociation of carbonic acid in seawater media. *Deep Sea Research part A.*
721 *Oceanographic Research Papers* 34, 10: 1733-1743.
722

723 Dickson A G (1990) Standard potential of the reaction: $\text{AgCl(s)} + \frac{1}{2}\text{H}_2(\text{g}) = \text{Ag(s)} + \text{HCl(aq)}$,
724 and the standard acidity constant of the ion HSO_4^- in synthetic sea water from 273.15 to
725 318.15 K. *Journal of Chemical Thermodynamics* 22: 113-127.
726

727 Duarte C M, Middleburg J J, and Caraco N (2005) Major role of marine vegetation on the
728 oceanic carbon cycle. *Biogeosciences* 2: 1-8.
729

730 Duarte C M, Marbà N, Gacia E, Fourqurean J W, Beggins J, Barrón C, and Apostolaki E T
731 (2010) Seagrass community metabolism: Assessing the carbon sink capacity of seagrass
732 meadows. *Global Biogeochemical Cycles* 24: GB4032, doi:10.1029/2010GB003793.
733

734 Fourqurean J W, Duarte C M, Kennedy H, Marbà N, Holmer M, Mateo M A, Apostolaki E T,
735 Kendrick G A, Krause-Jensen D, McGlathery K J, and Serrano O (2012) Seagrass
736 ecosystems as a globally significant carbon stock. *Nature Geoscience*: 505-509. DOI:
737 10.1038/NGEO1477
738

739 Frankignoulle M, and Bouquegneau J M (1990) Daily and Yearly Variation of total Inorganic
740 Carbon in a Productive Coastal Area. *Estuarine, Coastal and Shelf Science* 30: 79-89.
741

742 Gazeau F, Duarte C M, Gattuso J P, Barron C, Navarro N, Ruiz S, Prairie Y T, Calleja M,
743 Delille B, Frankignoulle M, and Borges A V (2005) Whole-system metabolism and CO_2
744 fluxes in a Mediterranean Bay dominated by seagrass beds (Palma Bay, NW
745 Mediterranean). *Biogeosciences* 2: 43-60.
746

747 Gleitz M, Rutgers van der Loeff M, Thomas D N, Dieckmann G S, and Millero F J (1995)
748 Comparison of summer and winter inorganic carbon, oxygen and nutrient concentrations in
749 Antarctic sea ice brines. *Marine Chemistry* 51: 81-91.
750

751 Goldman J C, and Brewer P G (1980) Effect of nitrogen source and growth rate on
752 phytoplankton-mediated changes in alkalinity. *Limnology Oceanography* 25: 352-357.

753
754 Gupta G V M, Sarma V V S S, Robin R S, Raman A V, Jai Kumar M, Rakesh M, and
755 Subramanian B R (2008) Influence of net ecosystem metabolism in transferring riverine
756 organic carbon to atmospheric CO₂ in a tropical coastal lagoon (Chilka Lake, India).
757 *Biogeochemistry* 87(3): 265-285.
758
759 Hill A E (1994) Fortnightly Tides in a Lagoon with Variable Choking. *Estuarine, Coastal and*
760 *Shelf Science* 38: 423-434.
761
762 Hopkinson C S, and Smith E M (2005) Estuarine respiration: an overview of benthic,
763 pelagic, and whole system respiration. *Respiration in Aquatic ecosystems* Chapter 8: 122-
764 146. Oxford University Press DOI:10.1093/acprof:oso/9780198527084.003.0008
765
766 Jiang Z P, Huang J C, Dai M, Kao S J, Hydes D J, Chou W C, and Jan S (2011) Short-term
767 dynamics of oxygen and carbon in productive nearshore shallow seawater systems of
768 Taiwan: Observations and modelling. *Limnology and Oceanography* 56, 5: 1832-1849.
769
770 Johnson R A, Gulick A G, Bolten A B, and Bjorndal K A (2017) Blue carbon stores in
771 tropical seagrass meadows maintained under green turtle grazing. *Nature: Scientific*
772 *reports*: 7 13545. DOI:10.1038/s41598-017-13142-4
773
774 Kennedy H, and Bjork M (2009) Seagrass Meadows. In: Laffoley D, and Grimsditch G *The*
775 *Management of Natural Coastal Carbon Sinks*: 23-29.
776
777 Kennedy H, Beggins J, Duarte C M, Fourqurean J W, Holmer M, Marbà N, and Middelburg
778 J J (2010) Seagrass sediments as a global carbon sink: Isotopic constraints. *Global*
779 *Biogeochemical Cycles* 24: 1-8.
780
781 Kjerfve B. (1986) Comparative Oceanography of Coastal lagoons. *Estuarine Variability*: 63-
782 81.
783
784 Koné M, Abril G, Kouadio K N, Delille B, and Borges A (2009) Seasonal variability of carbon
785 dioxide in the rivers and lagoons of Ivory Coast (West Africa). *Estuaries and Coasts* 32:
786 246-260. DOI: 10.1007/s12237-008-9121-0
787
788 Lazar B and Loya Y (1991) Bioerosion of coral reefs – A chemical approach. *Limnology and*
789 *Oceanography* 36: 377-383.
790
791 Lee K, Kim T W, Byrne R H, Millero F J, Feely R A, and Liu Y M (2010) The universal ratio
792 of boron to chlorinity for the North Pacific and North Atlantic oceans. *Geochimica et*
793 *Cosmochimica Acta* 74, 6: 1801-1811.
794

795 Le Quéré C, Andres R J, Boden T, Conway T, Houghton R A, House J I, Marland G, Peters
796 G P, van der Werf G R, Ahlström A, Andrew R M, Bopp L, Canadell J G, Ciais P, Doney S
797 C, Enright C, Friedlingstein P, Huntingford C, Jain A K, Jourdain C, Kato E, Keeling R F,
798 Klein Goldewijk K, Levis S, Levy P, Lomas M, Poulter B, Raupach M R, Schwinger J, Sitch
799 S, Stocker B D, Viovy N, Zaehle S, and Zeng N (2013) The global carbon budget 1959–
800 2011. *Earth System Science Data* 5, 1: 165-185. <https://doi.org/10.5194/essd-5-165-2013>.

801

802 Le Quéré, C., Andrew, R. M., Friedlingstein, P., Sitch, S., Pongratz, J., Manning, A. C.,
803 Korsbakken, J. I., Peters, G. P., Canadell, J. G., Jackson, R. B., Boden, T. A., Tans, P. P.,
804 Andrews, O. D., Arora, V. K., Bakker, D. C. E., Barbero, L., Becker, M., Betts, R. A., Bopp,
805 L., Chevallier, F., Chini, L. P., Ciais, P., Cosca, C. E., Cross, J., Currie, K., Gasser, T.,
806 Harris, I., Hauck, J., Haverd, V., Houghton, R. A., Hunt, C. W., Hurtt, G., Ilyina, T., Jain, A.
807 K., Kato, E., Kautz, M., Keeling, R. F., Klein Goldewijk, K., Körtzinger, A., Landschützer, P.,
808 Lefèvre, N., Lenton, A., Lienert, S., Lima, I., Lombardozzi, D., Metz, N., Millero, F.,
809 Monteiro, P. M. S., Munro, D. R., Nabel, J. E. M. S., Nakaoka, S.-I., Nojiri, Y., Padin, X. A.,
810 Peregón, A., Pfeil, B., Pierrot, D., Poulter, B., Rehder, G., Reimer, J., Rödenbeck, C.,
811 Schwinger, J., Séférian, R., Skjelvan, I., Stocker, B. D., Tian, H., Tilbrook, B., Tubiello, F.
812 N., van der Laan-Luijkx, I. T., van der Werf, G. R., van Heuven, S., Viovy, N., Vuichard, N.,
813 Walker, A. P., Watson, A. J., Wiltshire, A. J., Zaehle, S., and Zhu, D. (2018) Global Carbon
814 Budget 2017. *Earth Syst. Sci. Data* 10, 405-448, <https://doi.org/10.5194/essd-10-405-2018>.

815

816 Mehrbach C, Pytkowicz R M, Hawley J, Culberson C, and Barton B (1973) Measurements
817 of the apparent dissociation constants of carbonic acid in seawater at atmospheric
818 pressure. *MSc Thesis, Oregon State University, Corvallis*: Suelyn Williams.

819

820 Mørk E T, Sejr M K, Stæhr P A, and Sørensen L L (2016) Temporal variability of air-sea
821 CO₂ exchange in a low-emission estuary. *Estuarine, Coastal and Shelf Science* 176: 1-11.

822

823 Muduli P, Kanuri V V, Robin R S, Charan Kumar B, Patra S, Raman A V, Nageswarara Rao
824 G, and Subramanian B R (2012) Spatio-temporal variation of CO₂ emission from Chilka
825 Lake, a tropical coastal lagoon on the east coast of India. *Estuarine, Coastal and Shelf
826 Science* 113: 305-313.

827

828 Muduli P, Kanuri V V, Robin R S, Charan Kumar B, Patra S, Raman A V, Nageswarara Rao
829 G, and Subramanian B R (2013) Distribution of dissolved inorganic carbon and net
830 ecosystem production in a tropical brackish water lagoon, India. *Continental Shelf Research*
831 64: 75-87.

832

833 Neill S, Angeloudis A, Robins P, Walkington I, Ward S, Masters I, Lewis M, Piano M, Avdis
834 A, Piggott M, Aggidis G A, Evans P, Adcock T, Zidonis A, Ahmadian R, and Falconer R
835 (2018) Tidal range energy resource and optimization – past perspectives and future
836 challenges. *Renewable Energy* 127: 763-778. DOI: [10.1016/j.renene.2018.05.007](https://doi.org/10.1016/j.renene.2018.05.007)

837
838 Newton A, and Mudge S M (2005) Lagoon-sea exchanges, nutrient dynamics and water
839 quality management of the Ria Formosa (Portugal). *Estuarine, Coastal and Shelf Science*
840 62, 3: 405-414.

841
842 NIC (National Infrastructure Commission) *National Infrastructure Assessment technical*
843 *annex: Tidal power* (accessed Aug 8th, 2018) [https://www.nic.org.uk/wp-](https://www.nic.org.uk/wp-content/uploads/Tidal-power.pdf)
844 [content/uploads/Tidal-power.pdf](https://www.nic.org.uk/wp-content/uploads/Tidal-power.pdf)

845
846 NOAA (National Oceanic and Atmospheric Administration) *Trends in atmospheric carbon*
847 *dioxide* (accessed Aug 31st, 2013) <http://www.esrl.noaa.gov/gmd/ccgg/trends/global.html>

848
849 Orfila A, Jordi A, Basterretxea G, Vizoso G, Marba N, Duarte C M, Werner F E, and Tintor Æ
850 J (2005) Residence time and *Posidonia oceanica* in Cabrera Archipelago National Park,
851 Spain. *Continental Shelf Research* 25: 1339-1352 10.1016/j.csr.2005.01.004.

852
853 Papadimitriou S, Kennedy H, Rodrigues R M, Kennedy D P, and Heaton T H (2006) Using
854 variation in the chemical and stable isotopic composition of *Zostera noltii* to assess nutrient
855 dynamics in a temperate seagrass meadow. *Organic chemistry* 37: 1343-1358.

856
857 Papadimitriou S, Kennedy H A, Norman L, Kennedy D P, Dieckmann G S, and Thomas D N
858 (2012) The effect of biological activity, CaCO₃ mineral dynamics, and CO₂ degassing in the
859 inorganic carbon cycle in sea ice in late winter-early spring in the Weddell Sea, Antarctica.
860 *Journal of Geophysical Research* 117: 1-12.

861
862 Ribas-ribas M, Hernández-Ayón J M, Camacho-Ibar V F, Cabello-Pasini A, Mejia-Trejo A,
863 Durazo R, Galindo-Bect S, Souza A J, Forja J M, and Siqueiros-Valencia A (2011) Effects
864 of upwelling, tides and biological processes on the inorganic carbon system of a coastal
865 lagoon in Baja California. *Estuarine, Coastal and Shelf Science* 95: 367-376.

866
867 Robbins L L, Hansen M E, Kleypas J A, and Meylan S C (2010) CO₂calc: A user-friendly
868 seawater carbon calculator for Windows, Mac OS X, and iOS (iPhone). U.S. Geological
869 Survey, 17.

870
871 Roche R C, Walker-Springett K, Robins P E, Jones J, Veneruso G, Whitton T A, Piano M,
872 Ward S L, Duce C E, Waggitt J J, Walker-Springett G R, Neill S P, Lewis M J, and King J W
873 (2016) Research priorities for assessing potential impacts of emerging marine renewable
874 energy technologies: Insights from developments in Wales (UK). *Renewable Energy* 99:
875 1327-1341.

876

877 Rynne P, Reniers A, van de Kreeke J, and Macmahon J (2016) The effect of tidal exchange
878 on residence time in a coastal embayment. *Estuarine, Coastal and Shelf Science* 172.
879 10.1016/j.ecss.2016.02.001.
880
881 Sheldon J E, and Alber M (2006) The calculation of estuarine turnover times using
882 freshwater fraction and tidal prism models: A critical evaluation. *Estuaries and Coasts* 29, 1:
883 133-146.
884
885 Soetaert K, Hofmann A F, Middelburg J J, Meysman F J R, and Greenwodd J (2007) The
886 effect of biogeochemical processes on pH. *Marine Chemistry* 105: 30-51.
887
888 Takahashi T, Olafsson J, Goddard J G, Chipman D W, and Sutherland S C (1993)
889 Seasonal Variations of CO₂ and Nutrients in the High Latitude Surface Ocean: A
890 Comparative study. *Global Biogeochemical Cycles* 7: 843-878.
891
892 Takahashi T, Sutherland S C, Sweeney C, Poisson A, Metzl N, Tilbrook B, Bates N,
893 Wanninkhof R, Feely R A, Sabine C, Olafsson J, and Nojiri Y (2002) Global sea-air CO₂
894 flux based on climatological surface ocean pCO₂, and seasonal biological and temperature
895 effects. *Deep Sea Research Part II Topical Studies in Oceanography* 49: 1601-1622.
896 [https://doi.org/10.1016/S0967-0645\(02\)00003-6](https://doi.org/10.1016/S0967-0645(02)00003-6)
897
898 Tokoro T, Hosokawa S, Miyoshi E, Tada K, Watanabe K, Montani S, Kayanne H, and
899 Kuwae T (2014) Net uptake of atmospheric CO₂ by coastal submerged aquatic vegetation.
900 *Global Change Biology* 20(6): 1873-1884 doi: [10.1111/gcb.12543](https://doi.org/10.1111/gcb.12543)
901
902 Tsihrintzis V A, Sylaios G K, Sidiropoulou M, and Koutrakis E T (2007) Hydrodynamic
903 modeling and management alternatives in a Mediterranean, fishery exploited, coastal
904 lagoon. *Aquacultural Engineering* 36: 310-324.
905
906 Wang Z A, and Cai W J (2004) Carbon dioxide degassing and inorganic carbon export from
907 a marsh-dominated estuary (the Duplin River): A marsh CO₂ pump. *Limnol. Oceanogr.*
908 49(2), 341–354. <http://dx.doi.org/10.4319/lo.2004.49.2.0341>.
909
910 Wanninkhof R (1992) Relationship between wind speed and gas exchange over the ocean.
911 *Journal of Geophysical Research* 97, C5: 7373-7382.
912
913 Williams R G, and Fellows M J (2011) *Ocean Dynamics and the Carbon Cycle: Principles*
914 *and Mechanisms*. New York: Cambridge University Press.
915
916 Wolf-Gladrow D A, Zeebe R E, Klaas C, Körtzinger A, and Dickson A G (2007) Total
917 alkalinity: The explicit conservative expression and its application to biogeochemical
918 processes. *Marine Chemistry* 106: 287-300.

919

920 Zhai W D, Yan X L, and Qi D (2017) Biogeochemical generation of dissolved inorganic
921 carbon and nitrogen in the North Branch of inner Changjiang Estuary in a dry season.
922 *Estuarine, Coastal and Shelf Science* 197:136-149. DOI:
923 <http://dx.doi.org/10.1016/j.ecss.2017.08.027>.

924

925 Zouiten H, Diaz C A, Gomez A G, Cortezon J A R, and Alba J C (2013) An advanced tool
926 for eutrophication modeling in coastal lagoons: Application to the Victoria lagoon in the
927 north of Spain. *Ecological Modelling* 265: 99-113.

928

929 **Tables and Figures⁺**

930 ⁺Colour to be used for Figures except 2, 3 and 5.